Active Compliance Hybrid Zero Dynamics Control of Bounding on HyQ

Xin Liu, Claudio Semini and Ioannis Poulakakis

***Abstract*— This paper presents a control law that induces stable bounding on a model of the quadrupedal robot HyQ designed specifically for highly-dynamic locomotion. The controller integrates active compliance and torque planning with the framework of hybrid zero dynamics. Exploiting the hybrid nature of the system, the control action is developed in both continuous and discrete time to regulate the torques applied at the support leg and the motion of the swing leg. It is demonstrated that the proposed control law is capable of producing stable periodic bounding gaits. The controller is tested in simulations under different perturbations, including an unexpected vertical disturbance in ground height that amounts to 15% of the leg length, as well as under parameter uncertainty.**

I. Introduction

Robotic quadrupeds offer attractive solutions to applications that require enhanced mobility and versatility. A variety of sophisticated designs has been proposed to realize the potential of these robots in real-life applications. Focusing on quadrupeds specifically designed to run in a dynamically-stable manner, examples include Raibert's machines [1], Scout II [2], Tekken [3], KOLT [4], HyQ [5], BigDog [6], and Cheetah [7] which demonstrated outdoor mobility.

These robots employ various actuation and control schemes to implement different running gaits. Raibert and his collaborators used intuitive principles to make various symmetric gaits possible on a quadruped by generalizing one-foot gaits through the concept of virtual legs [1]. Along the same lines, the Scout II quadruped demonstrated efficient bounding gaits using only one actuator per leg located at the hip [2]. Dynamic walking and running motions were implemented on Tekken by combining explicit compliance with a neural oscillator network [3]. A different paradigm, employing fuzzy control informed by Raibert-style heuristics has been introduced in [8]. In connection with this work, the quadruped KOLT has been used to investigate running in [9], and a differential leg thrust controller has been applied to regulate trotting in [4]. Recently, an approach for controlling the torso dynamics of running quadrupeds based on optimally scaling the hip forces has been proposed in [7], [10].

Recent progress on bipedal walkers [11], and runners [12], suggest that established nonlinear control synthesis methods [13], suitably extended to accommodate the hybrid dynamics of legged locomotion [14], can be effective in stabilizing highly agile, dynamic locomotion on bipeds with complex morphologies. However, the design of controllers for running quadrupeds based on a rigorous formulation of the feedback control problem has not received much attention in the relevant literature. The differences in the morphology of the bipedal robots with that of the quadrupedal robots, could make the controllers developed for bipeds inapplicable on quadrupedal robots [12]. For example, the gravity of the torso in bipedal robot would only produces a small torque with respect to the hip axis. This is not the case for the quadruped, which has its torso horizontal and gravity produces a much larger torque. A direct application of the methods in [14] for quadruped would require large torque to actively stabilization of the torso for quadruped. On the other hand, this stabilization may not even be necessary for quadruped bounding gaits [1].

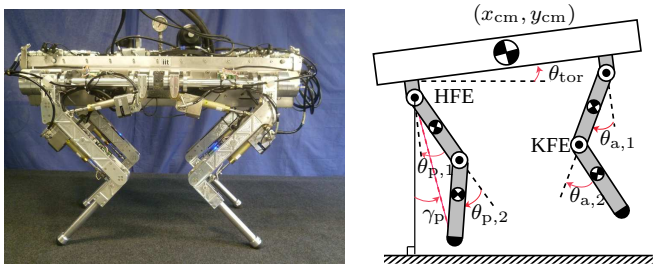

(a) (b)

Fig. 1. (a) The Hydraulic Quadruped HyQ. HyQ features three degrees of freedom per leg, two in the hip abduction/adduction and flexion/extension joints and one in the knee flexion/extension joint. (b) A sagittal plane model of HyQ used for the controller design.

In this paper, we propose a framework for control law design, that combines torque planning with established nonlinear control methods to obtain and stabilize periodic bounding gaits for quadrupeds. The controller harnesses the hybrid structure of the system by introducing control action in both continuous and discrete time. In continuous time, the controller "creates" a virtual spring at the knee of the support leg during the stance phases. In addition the continuous-time controller imposes virtual holonomic constraints on the leg that is in the air, reducing the dimension of the system on lower-dimensional, suitably parameterized, surfaces in the robot's state space. In discrete time, the parameters introduced by the continuous time controller are updated. The controller is tested in simulation using a sagittal-plane model of HyQ, demonstrating good performance in handling disturbances as well as parameter inaccuracy. A video with simulated bounding motions accompanies this paper.

Financial support by the European Union (European Social Fund-ESF) and Greek national funds through the Operational Program Education and Lifelong Learning of the National Strategic Reference Framework Research Funding Program: THALES: Reinforcement of the interdisciplinary and/or interinstitutional research & innovation is also acknowledged. This work is supported in part by NSF grant CMMI-1130372 and ARO contract W911NF-12-1-0117.

X. Liu and I. Poulakakis are with the Department of Mechanical Engineering, University of Delaware, DE, USA; {xinliu, poulakas}@udel.edu

C. Semini is with the Department of Advanced Robotics, Istituto Italiano di Tecnologia (IIT), Genova, Italy; claudio.semini@iit.it

The structure of this paper is as follows. Section II develops a bounding model of HyQ. Section III gives a detailed account on the controller design. Section IV implements the controller in simulation and Section V concludes the paper.

II. Modeling Bounding with HyQ

In this section, a mathematical model of the quadrupedal robot HyQ (Hydraulic Quadruped) shown in Fig. 1(a) in bounding is developed. HyQ is a fully torque-controlled robot built by the Dynamic Legged Systems Lab of the Istituto Italiano di Tecnologia (IIT) [5]. The robot weighs about 86kg in its current configuration and has a height of 1m with fully extended legs. Each leg has three degrees of freedom: two in the hip (abduction/adduction (HAA) and flexion/extension (HFE)) and one in the knee (flexion/extension (KFE)). High-performance servovalves enable joint-level torque and position control with excellent tracking [15]. The high power-density of hydraulic actuators allow strong and fast leg motions. The robustness of hydraulic actuation against impact also makes HyQ a very suitable platform for dynamic gaits, such as trotting and bounding.

In modeling bounding with HyQ, it is assumed that the essential features of the robot's motion take place in the sagittal plane, resulting in the planar model of Fig. 1(b). In this model, the four leg abduction-adduction degrees of freedom are not considered. In Fig. 1(b), the back and front virtual legs represent the collective effect of the back and front physical leg pairs, respectively. The geometric and inertia parameters of the model can be found in Table I.

TABLE I
Mechanical Parameters of the Model

Parameter	Value	Units
Torso mass (including HAA joints)	72.00	kg
Upper leg mass (virtual leg)	5.30	kg
Lower leg mass (virtual leg)	1.60	kg
Total Mass	85.80	kg
Torso Inertia (including HAA joints)	6.98	kg m^2
Upper leg inertia	0.05	kg m^2
Lower leg inertia	0.02	kg m^2
Hip-to-Hip distance	0.74	m
HAA linkage length	0.12	m
Upper leg linkage length	0.35	m
Lower leg linkage length	0.33	m
Upper leg COM to hip distance	0.162	m
Lower leg COM to knee distance	0.122	m

Depending on the foot in contact with the ground, the model can be in one of the following phases: flight "f," anterior stance "sa," posterior stance "sp," and double stance "sd". Figure 2 shows the phase sequence of a *nominal* bounding gait, which does not include a double stance phase; however, in converging from perturbations, the model can go through double stance phases. The indices "sw" and "su" refer to the swing leg and the support leg respectively. Furthermore, quantities related to the hip and knee joints, such as torques and angles, will be denoted by "1" and "2," respectively.

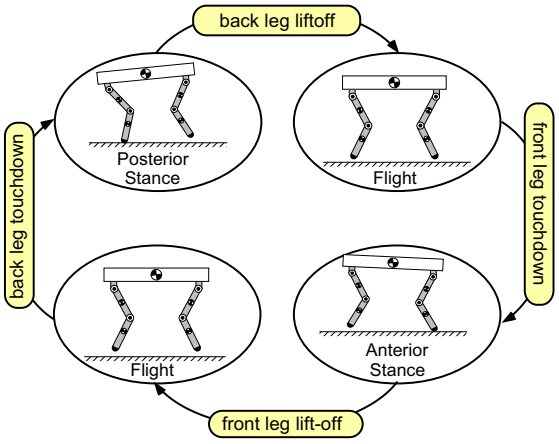

Fig. 2. Phase transition of a nominal bounding gait.

A. Dynamics in Floating-base Form

As defined in Fig. 1(b), a convenient choice of generalized coordinates describing the model's configuration is $q := (x_{\mathrm{cm}}, y_{\mathrm{cm}}, \theta_{\mathrm{tor}}, \theta_{\mathrm{p},1}, \theta_{\mathrm{p},2}, \theta_{\mathrm{a},1}, \theta_{\mathrm{a},2})'$. The dynamics can be written in the form

$$D(q)\ddot{q} + C(q,\dot{q})\dot{q} + G(q) = Bu + J^T F_{\mathrm{ext}}, \qquad (1)$$

where D is the mass matrix, C contains Coriolis and centrifugal terms, G is the vector of gravity-dependent forces, and B is the matrix mapping the input vector $u := (u_{\mathrm{p},1}, u_{\mathrm{p},2}, u_{\mathrm{a},1}, u_{\mathrm{a},2})'$ to the vector of generalized forces. In (1), $J := \left(J^{x\prime}, J^{y\prime}\right)'$ is the contact Jacobian obtained by differentiating the position of the foot with respect to an inertia frame, while $F_{\mathrm{ext}} = (F^x_{\mathrm{ext}}, F^y_{\mathrm{ext}})'$ is the interaction force, which is zero when the toe is in flight.

The contact between the toe and the ground is modeled based on a Coulomb friction model, resulting in

$$J^y\ddot{q} + \dot{J}^y\dot{q} = 0 \qquad (2)$$

$$J^x\ddot{q} + \dot{J}^x\dot{q} = 0 \quad \text{or} \quad F^x_{\mathrm{ext}} = \mu F^y_{\mathrm{ext}} \qquad (3)$$

that are augmented to (1) to solve for $\ddot{q}$ and F_{ext}; in (3), μ is the sliding friction coefficient assumed to be 0.8. Depending on whether sliding occurs, either constraint in (3) is used.

B. Reduced Dynamics

In the anterior and posterior stance phases, and under the assumption that the toe does not slide over the ground, the equations of motion can be written as:

$$D_i(q_{\mathrm{s}})\ddot{q}_{\mathrm{s}} + C_i(q_{\mathrm{s}},\dot{q}_{\mathrm{s}})\dot{q}_{\mathrm{s}} + G_i(q_{\mathrm{s}}) = B_i u \ , \qquad (4)$$

for $i \in \{\mathrm{sa}, \mathrm{sp}\}$, where the configuration variables are $q_{\mathrm{s}} := (\theta_{\mathrm{tor}}, \theta_{\mathrm{p},1}, \theta_{\mathrm{p},2}, \theta_{\mathrm{a},1}, \theta_{\mathrm{a},2})'$.

C. Transitions

For bounding gaits, transitions among phases are triggered by touchdown (TD) or liftoff (LO) events.

1) Flight-to-stance Transition: Switching from flight to the anterior or posterior stance, or from the anterior or posterior stance to double stance, occurs at TD, which is modeled as a completely inelastic impact that results in no rebound according to the assumptions listed in [14, Section 3.4]. Note that the resulting impact maps leave the configuration variables unaffected, while the corresponding velocities experience jumps.

2) Stance-to-flight Transition: The robot enters the flight phase when the support leg takes off. This event is characterized by the zeroing of the normal component of the ground reaction force. With the knee and hip joints actively controlled, the liftoff event can be initiated by actively flexing the joints. Hence, we will assume that the legs take off when the corresponding knee joint angle is $\pm 40^\circ$, where "$+$" refers to the posterior and "$-$" to the anterior leg.

III. Controller Design

The proposed controller – see Fig. 3 for an overview of the control action – is largely inspired by the study of passive bounding gaits. By commanding appropriate leg touchdown angles at flight phases, and keeping the leg passive during the stance phases, self-stable periodic bounding gaits can be generated by low-dimension models with mass-less springy legs [16]. HyQ, however, is neither energy-conservative nor has any springs in it. Hence, to "mimic" the behavior of the passive model the knee joint of the support leg is torque-controlled to create a virtual spring while (virtual) holonomic constraints are imposed on the joints of the swing leg so that it lands with a preferred touchdown angle. Furthermore, in contrast to the passive hip joints of the low-dimensional models, the hip joint of the support leg is torque-controlled to compensate for energy losses. The imposed holonomic constraints introduce parameters that are updated in a discrete time to render the constraints impact-invariant, leading to the notion of hybrid zero dynamics.

A. Stance Phase Torque Planning and Motion Control

The stance phase dynamics (4) can be written as

$$\dot{x}_{\rm s} = f_i(x_{\rm s}) + g_i^{\rm su}(x_{\rm s})u_i^{\rm su} + g_i^{\rm sw}(x_{\rm s})u_i^{\rm sw}, \tag{5}$$

where $i \in \{\rm sa, sp\}$ and $x_{\rm s} := (q_{\rm s}', \dot{q}_{\rm s}')'$ is the state vector.

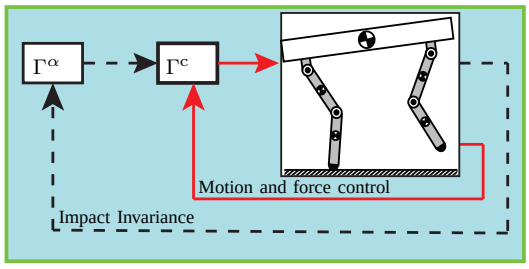

Fig. 3. Feedback diagram illustrating the structure of the controller. The continuous line represents signals in continuous time; the dashed lines represent signals in discrete time. The continuous-time controller $\Gamma^{\rm c}$ creates an actively compliant zero dynamics using torque planning and motion control. The discrete-time controller Γ^{α} updates parameters to ensure invariance under the transition maps.

The purpose of the controller at stance phases is to indirectly "shape" the force exerted by the support leg on the ground, and to place the swing leg at a desired configuration. To achieve these objectives, a combination of torque planning and motion control is employed.

1) Active Compliance through Torque Planning for the Support Leg: To regulate the interaction between the torso and the environment, the controller commands desired torque profiles at the hip and knee joints of the leg in contact with the ground. In more detail, a constant torque β_i, $i \in \{\rm sp, sa\}$ is commanded at the hip actuator of the support leg as

$$u_{\rm p,1} = \beta_{\rm sp} \text{ and } u_{\rm a,1} = \beta_{\rm sa} \tag{6}$$

for the stance-posterior and the stance-anterior phase. Next, the following torque is commanded at the knee joint

$$u_{\rm p,2} = \bar{u}_{\rm p,2} + k_{\rm p}(\theta_{\rm p,2} - \bar{\theta}_{\rm p,2}) \tag{7}$$

for the stance-posterior phase, and similarly

$$u_{\rm a,2} = \bar{u}_{\rm a,2} + k_{\rm a}(\theta_{\rm a,2} - \bar{\theta}_{\rm a,2}) \tag{8}$$

for the stance-anterior phase. In (7), $k_{\rm p}$ and $\bar{\theta}_{\rm p,2}$ are the stiffness and the rest angle of the virtual knee spring for the posterior leg in the posterior-stance phase; similarly, $k_{\rm a}$ and $\bar{\theta}_{\rm a,2}$ in (8) are the corresponding constants for the anterior leg virtual spring in the anterior-stance phase. We require $\bar{\theta}_{\rm p,2} = -\bar{\theta}_{\rm a,2} = 40^\circ$, consistent with the liftoff conditions in II-C so that the (virtual) spring is completely undeformed at liftoff. Note that the offsets $\bar{u}_{\rm p,2}$ and $\bar{u}_{\rm a,2}$ in (7) and (8), are added to ensure that the normal component of the ground reaction force is sufficiently large to prevent toe slipping.

To summarize, for each $i \in \{\rm sp, sa\}$, the commanded torque profiles for the support leg during the stance-posterior and stance-anterior phases, can be written in the form

$$u_i^{\rm su} = \Gamma_i^{\rm su}(x_{\rm s}, \alpha_i^{\rm su}) \tag{9}$$

for $i \in \{\rm sp, sa\}$, where $\alpha_{\rm sp}^{\rm su} := \{\bar{u}_{\rm p,2}, k_{\rm p}, \beta_{\rm sp}\}$ and $\alpha_{\rm sa}^{\rm su} := \{\bar{u}_{\rm a,2}, k_{\rm a}, \beta_{\rm sa}\}$. With this notation, the stance dynamics (5) for $i \in \{\rm sp, sa\}$ in closed loop with the controller of the corresponding support leg (9) becomes

$$\dot{x}_i = f_i^{\rm sw}(x_{\rm s}, \alpha_i^{\rm su}) + g_i^{\rm sw}(x_{\rm s})u_i^{\rm sw}, \tag{10}$$

where $f_i^{\rm sw}(x_{\rm s}, \alpha_i^{\rm su}) := f_i(x_{\rm s}) + g_i^{\rm su}(x_{\rm s})\Gamma_i^{\rm su}(x_{\rm s}, \alpha_i^{\rm su})$. Note that at double stance, both legs are support legs and are torque-controlled using the controller described above.

2) Swing Leg Motion Control: The continuous-time control input $u^{\rm sw}$ in (10) includes the hip and knee joint torques of the swing leg, and it will be used to prepare the swing leg for its ensuing touchdown. To achieve this objective, we associate to (10) the output

$$y_i = h_i(q_{\rm s}, \alpha_i^{\rm sw}) := H_i q_{\rm s} - h_i^{\rm d}(s_i(q_{\rm s}), \alpha_i^{\rm sw}) \tag{11}$$

for $i \in \{\rm sp, sa\}$, where $H_i q_{\rm s}$ is the vector of the controlled variables, which contains the absolute hip angle and the knee angle relative to the upper part of the swing leg; i.e.,

$$H_{\rm sp} := \begin{bmatrix} 1 & -1 & 0 & 0 & 0 \\ 0 & 0 & 1 & 0 & 0 \end{bmatrix} \text{ and } H_{\rm sa} := \begin{bmatrix} 1 & 0 & 0 & -1 & 0 \\ 0 & 0 & 0 & 0 & 1 \end{bmatrix} \tag{12}$$

for the stance-posterior and the stance-anterior phases.

In (11), $h_i^{\rm d}$ is the desired evolution of the controlled variables, which is represented by smooth polynomials as detailed in the Appendix. We only mention here that the polynomials are parameterized by the normalized variables

$$s_{\rm sp}(q_{\rm sp}) := \frac{\gamma_{\rm p}(q_{\rm sp}) - \gamma_{\rm p}^{\rm td}}{\Delta_{\rm sp}} \quad \text{and} \quad s_{\rm sa}(q_{\rm sa}) := \frac{\gamma_{\rm a}(q_{\rm sa}) - \gamma_{\rm a}^{\rm td}}{\Delta_{\rm sa}} \tag{13}$$

where $\Delta_{\rm sp}$ and $\Delta_{\rm sa}$ are constants, $\gamma_{\rm p}$ and $\gamma_{\rm a}$ are the angles between the vertical and the line connecting the hip with the foot of the posterior and anterior leg, respectively, and $\gamma_{\rm p}^{\rm td}$, $\gamma_{\rm a}^{\rm td}$ are the corresponding values at touchdown; see Fig. 1(b). Note that, for each $i \in \{\rm sp, sa\}$, s_i is a monotonic function of the configuration variables, essentially replacing time in the parameterization of the polynomials described in the Appendix. Finally, all the parameters associated with the design of the desired evolution $h_i^{\rm d}$ of the controlled variables, are collected in the array $\alpha_i^{\rm sw}$, which, participates in the definition of the constraint (11).

The outputs (11) are functions of the configuration variables only; hence, they can be interpreted as holonomic constraints, which can be imposed (asymptotically) on the system by driving (11) to zero. To do so, we differentiate (11) for given values of $\alpha_i := \{\alpha_i^{\rm su}, \alpha_i^{\rm sw}\}$ to get[1]

$$\frac{d^2 y_i}{dt^2} = L^2_{f_i^{\rm sw}} h_i(x_{\rm s}, \alpha_i) + L_{g_i^{\rm sw}} L_{f_i^{\rm sw}} h_i(x_{\rm s}, \alpha_i) u^{\rm sw} \tag{14}$$

where $L_{g_i^{\rm sw}} L_{f_i^{\rm sw}} h_i(x_{\rm s}, \alpha_i)$ is the decoupling matrix. Upon verifying the invertibility of $L_{g_i^{\rm sw}} L_{f_i^{\rm sw}} h_i(x_{\rm s}, \alpha_i)$,

$$u_*^{\rm sw}(x_{\rm s}, \alpha_i) := -\left(L_{g_i^{\rm sw}} L_{f_i^{\rm sw}} h_i(x_{\rm s}, \alpha_i)\right)^{-1} L^2_{f_i^{\rm sw}} h_i(x_{\rm s}, \alpha_i) \tag{15}$$

is the unique control input which renders the surface

$$\begin{aligned} \mathcal{Z}_{\alpha_i} := \{ & x_{\rm s} \in \mathcal{X}_i \mid h_i(q_{\rm s}, \alpha_i^{\rm sw}) = 0, \\ & L_{f_i^{\rm sw}} h_i(x_{\rm s}, \alpha_i) = 0 \} \end{aligned} \tag{16}$$

invariant under the flow of the closed-loop dynamics. Zeroing the output effectively reduces the dimension of the system by restricting its dynamics on the zero dynamics surface $\mathcal{Z}_{\alpha_i}$. The dynamics of the system restricted on $\mathcal{Z}_{\alpha_i}$,

$$\dot{z} = f_i^*|_{\mathcal{Z}_{\alpha_i}}(z) \tag{17}$$

is the corresponding zero dynamics. To ensure attractivity of $\mathcal{Z}_{\alpha_i}$, the input (15) is modified as

$$\begin{aligned} u^{\rm sw} &= \Gamma_i^{\rm sw}(x_{\rm s}, \alpha_i) \\ &= \left(L_{g_i^{\rm sw}} L_{f_i^{\rm sw}} h_i(x_{\rm s}, \alpha_i)\right)^{-1} \\ &\quad \left[\upsilon(y_i, \dot{y}_i, \epsilon) - L_{g_i^{\rm sw}} L_{f_i^{\rm sw}} h_i(x_{\rm s}, \alpha_i)\right] \end{aligned} \tag{18}$$

where

$$\upsilon(y_i, \dot{y}_i, \epsilon) := -\frac{1}{\epsilon^2} K_{\rm P} y_i - \frac{1}{\epsilon} K_{\rm V} \dot{y}_i, \tag{19}$$

and $K_{\rm P}$, $K_{\rm V}$ are gain matrices, and $\epsilon > 0$. Under the influence of the continuous-time feedback laws $\Gamma_i^{\rm sw}$ for $i \in \{\rm sp, sa\}$ the solutions of (10) converge to the invariant surface $\mathcal{Z}_{\alpha_i}$ exponentially fast.

In what follows, the combined continuous-time control action during the stance phases $i \in \{\rm sp, sa\}$ will be denoted by $\Gamma_i^{\rm c} = \{\Gamma_i^{\rm su}, \Gamma_i^{\rm sw}\}$, depicted in Fig. 3.

B. Flight Phase Motion Control

The continuous-time control design in the flight phases is analogous to that of the stance, thus the exposition here will be terse. Let $x_{\rm f} := (q', \dot{q}')'$ be the state for the flight phase. Then, the dynamics in both flight phases can be written as

$$\dot{x}_{\rm f} = f_{\rm f}(x_{\rm f}) + g_{\rm f}(x_{\rm f}) u. \tag{20}$$

To allow the use of polynomials with different coefficients in defining the desired evolution of the controlled variables, to each flight phase – that is, the flight phase after the posterior leg liftoff denoted by the index $\rm f_1$, and the flight phase after the anterior leg liftoff denoted by $\rm f_2$ – we associate the output

$$y_i = h_i(x_{\rm f}, \alpha_i) := H_{\rm f} q - h_i^{\rm d}(s_{\rm f}(q), \alpha_i), \tag{21}$$

where $i \in \{\rm f_1, f_2\}$. In (21), the controlled variables $H_{\rm f} q$ are the same in both flight phases, and correspond to the absolute hip and the relative knee angles of the posterior and anterior legs; that is, $H_{\rm f}$ is defined as

$$H_{\rm f} := \begin{bmatrix} \mathbf{0}_{2\times 2} & H_{\rm sp} \\ \mathbf{0}_{2\times 2} & H_{\rm sa} \end{bmatrix}. \tag{22}$$

In (21), for each flight phase $i \in \{\rm f_1, f_2\}$, $h_i^{\rm d}$ represents the desired evolution of the controlled variables, which is defined by smooth polynomials parameterized through the monotonic quantity

$$s_i(q_i) = \frac{x_{\rm cm} - x_{{\rm cm},i}^{\rm lo}}{\Delta_i}, \tag{23}$$

where Δ_i is a normalizing constant, and $x_{{\rm cm},i}^{\rm lo}$ is the value of the horizontal coordinate $x_{\rm cm}$ of the torso's COM at liftoff, so that (23) represents a monotonically increasing quantity that replaces time in the parameterization of the polynomials. The details associated with the polynomials are presented in the Appendix; we only mention here that α_i are the parameters associated with the construction of $h_i^{\rm d}$ in each flight phase $i \in \{\rm f_1, f_2\}$.

To impose the constraints, a continuous-time controller that zeros the output (21) is designed. The process is similar to the one employed in the stance phase. In each phase $i \in \{\rm f_1, f_2\}$, the corresponding controller has the form

$$\begin{aligned} u \ &= \Gamma_i^{\rm c}(x_{\rm f}, \alpha_i) \\ &:= \left(L_{g_{\rm f}} L_{f_{\rm f}} h_i(x_{\rm f}, \alpha_i)\right)^{-1} \left[\upsilon(y_i, \dot{y}_i, \epsilon) - L_{g_{\rm f}} L_{f_{\rm f}} h_i(x_{\rm f}, \alpha_i)\right]. \end{aligned} \tag{24}$$

where the auxiliary control input υ has the same form with (19), and it renders the zero dynamics surface

$$\mathcal{Z}_{\alpha_i} = \{x_{\rm f} \in \mathcal{X}_{\rm f} \mid h_i(q_{\rm f}, \alpha_i) = 0, L_{f_{\rm f}} h_i(x_{\rm f}, \alpha_i) = 0\} \tag{25}$$

invariant and attractive.

[1]Note that the output (11) depends only on $\alpha_i^{\rm sw}$; however, when we differentiate along the dynamics (10) the resulting Lie derivatives depend also on the parameters $\alpha_i^{\rm su}$ introduced by the force controller.

C. Discrete-time Control Laws

At discrete transitions, zeroing of the output may be violated when $x_i^+ \notin \mathcal{Z}_{\alpha_i}$ for $i \in \{\mathrm{sp}, \mathrm{sa}, \mathrm{f}_1, \mathrm{f}_2\}$. To ensure that the zero dynamics surface in each phase is invariant under transitions, the control action updates the parameters α_i according to controllers

$$\alpha_i^+ = \Gamma_i^\alpha(x_i^+) \tag{26}$$

for $i \in \{\mathrm{sp}, \mathrm{sa}, \mathrm{f}_1, \mathrm{f}_2\}$ as detailed in the Appendix.

IV. Simulation Results

The bounding gait naturally defines a Poincaré return map. We select the Poincaré section to be the flight-to-stance-posterior switching surface $\mathcal{S}_{\mathrm{f}_2 \to \mathrm{sp}}$, when the posterior leg touches the ground. The corresponding Poincaré map $\mathcal{P} : \mathcal{S}_{\mathrm{f}_2 \to \mathrm{sp}} \to \mathcal{S}_{\mathrm{f}_2 \to \mathrm{sp}}$ of the system under the influence of the combined continuous-time controllers Γ_i^{c} and the discrete-time controllers Γ_i^α, with $i \in \{\mathrm{sp}, \mathrm{sa}, \mathrm{sd}, \mathrm{f}_1, \mathrm{f}_2\}$ becomes

$$x_{\mathrm{sp}}^+[k+1] = \mathcal{P}\left(x_{\mathrm{sp}}^+[k]\right) \tag{27}$$

where $x_{\mathrm{sp}}^+[k]$ is the state after the k-th impact of the posterior leg with the ground. Then, a nominal periodic running gait corresponds to a fixed point of the Poincaré return map defined by

$$x_{\mathrm{sp}}^+ = \mathcal{P}\left(x_{\mathrm{sp}}^+\right) \tag{28}$$

By using Matlab's `fsolve`, a number of fixed points can be computed for (28). In particular, a fixed point corresponding to an average horizontal velocity 2.527m/s is analyzed here. Numerical computations reveal that the norm of the dominant eigenvalue of the linearized Poincaré map (28) at this fixed point is 0.95, implying local exponential stability. Note that the resulting nominal motion has neither double stance phase nor slip of the foot.

To demonstrate the performance of the controller, we consider the case where the model experiences an unexpected variation in the ground height of $9\mathrm{cm}$, which is approximately equal to 15% of the leg length. Figures 4(a) and 4(b) present the evolution of the torso height and the horizontal velocity, showing convergence to the nominal gait. The corresponding continuous-time inputs are presented in Figs. 4(c) and 4(d), illustrating that the peak torques are well within the capabilities of the hydraulic actuators of the robot.

Figure 5 presents a numerical estimate of the domain of attraction of this controller in the $(\dot{x}_{\mathrm{cm}}, y_{\mathrm{cm}})$ plane. The disturbance is added at the end of the stance-posterior phase. The blue area is the part where the robot eventually converges back to the original fixed point. Note that the largest portion of the region of attraction lies in the second quadrant, where the vertical displacement of the robot is increased while the velocity is decreased; this is due to the fact that such disturbances do not drastically increase the total energy of the system, and can be rejected relatively easily.

Finally, Fig. 6 presents the sensitivity of the controller to the inaccuracy in the inertia parameters. Here it is assumed that the mass of the thigh and shank has an inaccuracy randomly distributed within $\pm 30\%$ of the model, while the torso mass and moment of inertia is either increased or decreased by 20% (corresponding to 14kg and 1.4kg-m^2). For all the points randomly tested, the controller is able to converge to a periodic gait. Notice that due to the underactuation of the system, the robot will not return to the nominal periodic gait, but it will converge to a nearby orbit.

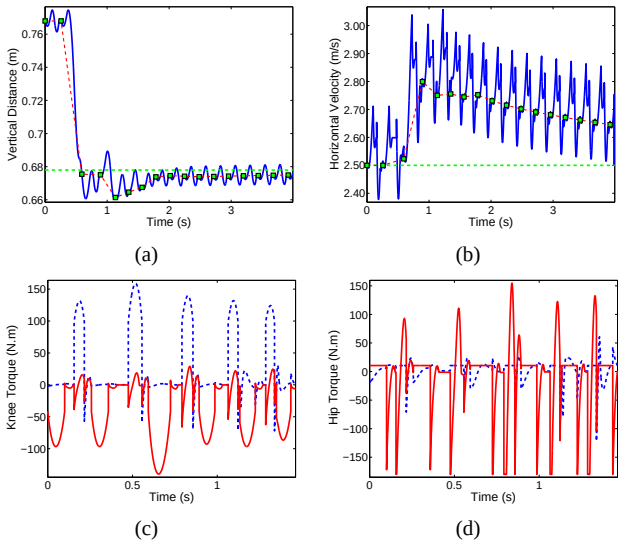

Fig. 4. Response of the system to a $9\mathrm{cm}$ step-down disturbance showing convergence to the nominal orbit. (a) Hopping height; (b) forward velocity; (c) knee joint actuator torque; (d) hip joint actuator torque. In (a) and (b), the green squares denote the state at Poincare section. In (c) and (d), the red lines correspond to the posterior leg and the blue dashed lines to the anterior leg torques.

V. Conclusion

This paper proposes a framework for designing controllers that integrate actively generated compliance and torque planning with motion control to induce dynamically-stable bounding gaits on a model of HyQ. In continuous time the purpose of the controller is twofold. First, it commands suitably parameterized torque profiles to the support leg actuators to create active compliance and to compensate for energy loss. Second, it enforces a set of (virtual) holonomic constraints to restrict the evolution of the hip and knee angles on lower-dimensional surfaces in the state space of

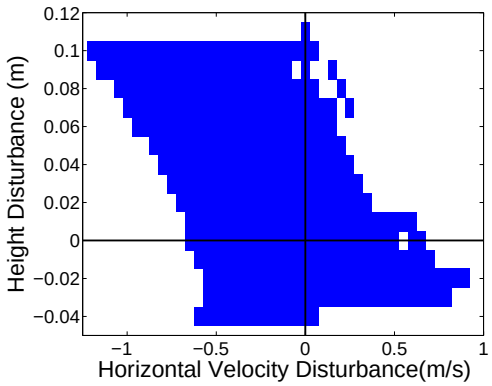

Fig. 5. An estimate of the region of attraction. The blue area represents states that can be accommodated by the controller.

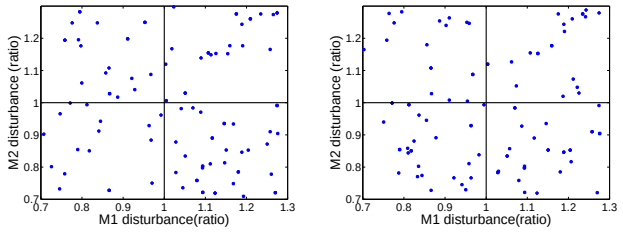

(a) (b)

Fig. 6. Robustness test. The leg mass M_1 and M_2 is randomly perturbed within $\pm 30\%$ of the nominal value. All the points randomly checked stabilized to periodic gaits. The torso mass and moment of inertia is increased by 20% (a) and decreased by 20% (b).

the system. The parameters introduced through continuous-time control are updated by the discrete-time controller, which effectively re-plans the constraint profiles providing additional control action. Aiming at experimentally verifying the proposed control method on HyQ, the controller is tested in simulation under different disturbances, including unanticipated ground height variation, horizontal velocity, as wells as parameter inaccuracy.

APPENDIX

This appendix provides more details on the design of the polynomials that characterize the desired evolution of the controlled variables. To simplify the presentation, we focus on a single controlled variable θ with desired evolution h_θ^{d}.

1) Polynomial Design: We consider the output

$$y = \theta - h_\theta^{\mathrm{d}}(s(q), \alpha), \tag{29}$$

where s is a monotonic function of q, defined though $s(q) = \frac{\phi(q)-\phi_0}{\Delta}$ with ϕ_0 and Δ suitably selected constants that have the meaning of the constants participating in (13) for the stance and in (23) for the flight phases. For example, in the stance-posterior phase, ϕ is γ_{p}, ϕ_0 is $\gamma_{\mathrm{p}}^{\mathrm{td}}$ and Δ corresponds to Δ_{sp}. Then, h_θ^{d} is selected as

$$h_\theta^{\mathrm{d}}(s(q)) := \begin{cases} \displaystyle\sum_{k=0}^{4} a_k s(q)^k, & \text{if } s < \sigma \\ a_5, & \text{if } s \geq \sigma. \end{cases} \tag{30}$$

The first part of (30) transfers the corresponding controlled variable θ over the interval $[0, \sigma)$ to its target position with zero final velocity and acceleration. The second part of (30) keeps the controlled variable equal to constant a_5 until the phase terminates. Lastly, to ensure continuity up to the second derivative, we impose the following constraints

$$\begin{aligned} a_4\sigma^4 + \ a_3\sigma^3 + \ a_2\sigma^2 + \ a_1\sigma + \ a_0 &= a_5 \\ 4a_4\sigma^3 + 3a_3\sigma^2 + 2a_2\sigma + \ a_1 &= 0 \\ 12a_4\sigma^2 + 6a_3\sigma + 2a_2 &= 0. \end{aligned} \tag{31}$$

For each output (two for the stance phase and four for the flight phases), this procedures introduces a number of parameters – namely, $\{a_0, ..., a_5, \sigma, \Delta, \phi_0\}$ – which participate in the definition of α in (29).

2) Coefficient Updates for Invariance: To extend invariance in the hybrid setting we need to ensure that the initial condition x_i^+ for each phase belongs on the corresponding zero dynamics surface $\mathcal{Z}_{\alpha_i}$, where the (possible) dependence of $\mathcal{Z}$. To satisfy this condition, the surface $\mathcal{Z}_{\alpha_i}$ can be "deformed" by updating α_i so that $x_i^+ \in \mathcal{Z}_{\alpha_i}$. Consider again the controlled variable θ, and let θ^+ be its initial value. Then, updating the coefficients in (30) through

$$a_0 = \theta^+ \quad \text{and} \quad a_1 = (1/\dot{s})\dot{\theta}^+, \tag{32}$$

for all the controlled variables ensures invariance under transitions. Note that (31) and (32) define a system of five equations with five unknowns, the solution of which provides the polynomial coefficients.

REFERENCES

[1] M. H. Raibert, *Legged Robots that Balance*. Cambridge, MA: MIT Press, 1986.

[2] I. Poulakakis, J. Smith, and M. Buehler, "Modeling and experiments of untethered quadrupedal running with a bounding gait: The Scout II robots," *The International Journal of Robotics Research*, vol. 24, no. 4, pp. 239–256, 2005.

[3] Y. Fukuoka, H. Kimura, and A. H. Cohen, "Adaptive dynamic walking of a quadruped robot on irregular terrain based on biological concepts," *The International Journal of Robotics Research*, vol. 23, no. 10-11, pp. 1059–1073, 2004.

[4] J. Estremera and K. Waldron, "Thrust control, stabilization and energetics of a quadruped running robots," *The International Journal of Robotics Research*, vol. 27, no. 10, p. 1135, 2008.

[5] C. Semini, N. G. Tsagarakis, E. Guglielmino, M. Focchi, F. Cannella, and D. G. Caldwell, "Design of HyQ - a hydraulically and electrically actuated quadruped robot," *Proceedings of the IMechE Part I: Journal Systems and Control Engineering*, vol. 225, no. 6, pp. 831–849, 2011.

[6] M. Raibert, K. Blankespoor, G. Nelson, R. Playter, and the BigDog Team, "BigDog, the Rough-Terrain Quadruped Robot," in *Proceedings of the 17th IFAC World Congress*, Seoul, Korea, July 2008, pp. 10 822–10 825.

[7] H.-W. Park and S. Kim, "Quadrupedal galloping control for a wide range of speed via vertical impulse scaling," *Bioinspiration & Biomimetics*, vol. 10, no. 2, p. 025003, Mar. 2015.

[8] D. Marhefka, D. Orin, J. Schmiedeler, and K. Waldron, "Intelligent control of quadrupedal gallops," *IEEE/ASME Transactions on Mechatronics*, vol. 8, no. 4, pp. 446–456, 2003.

[9] J. Nichol, S. Singh, K. Waldron, L. Palmer, and D. Orin, "System Design of a Quadrupedal Galloping Machines," *The International Journal of Robotics Research*, vol. 23, no. 10-11, p. 1013, 2004.

[10] A. K. Valenzuela and S. Kim, "Optimally scaled hip-force planning: A control approach for quadrupedal running," in *Proceedings of the IEEE International Conference on Robotics and Automation*, 2012, pp. 1901–1907.

[11] K. Sreenath, H. Park, I. Poulakakis, and J. Grizzle, "A compliant hybrid zero dynamics controller for stable, efficient and fast bipedal walking on MABEL," *The International Journal of Robotics Research*, vol. 30, no. 9, pp. 1170–1193, 2011.

[12] ——, "Embedding active force control within the compliant hybrid zero dynamics to achieve stable, fast running on MABEL," *The International Journal of Robotics Research*, vol. 32, no. 3, pp. 324–345, Mar. 2013.

[13] A. Isidori, *Nonlinear Control Systems*, 3rd ed. Berlin: Springer-Verlag, 1995.

[14] E. R. Westervelt, J. W. Grizzle, C. Chevallereau, J. H. Choi, and B. Morris, *Feedback Control of Dynamic Bipedal Robot Locomotion*. Taylor & Francis/CRC Press, 2007.

[15] T. Boaventura, C. Semini, J. Buchli, M. Frigerio, M. Focchi, and D. G. Caldwell, "Dynamic torque control of a hydraulic quadruped robot," in *IEEE International Conference in Robotics and Automation (ICRA)*, 2012, pp. 1889–1894.

[16] I. Poulakakis, E. G. Papadopoulos, and M. Buehler, "On the stability of the passive dynamics of quadrupedal running with a bounding gait," *The International Journal of Robotics Research*, vol. 25, no. 7, pp. 669–687, 2006.